Modelling of the Calendering Process of NMC-622 Cathodes in Battery Production Analyzing Machine/Material–Process–Structure Correlations

David Schreiner,* Maximilian Oguntke, Till Günther, and Gunther Reinhart

The shift in the transport sector from internal combustion engines to battery-powered electric vehicles and the continued demand for portable applications increases the need for batteries in the coming years. To optimize battery technologies, it is essential to fully understand the production process and the associated parameters as well as their influence on the chemical processes within the cell. At the Institute for Machine Tools and Industrial Management (iwb), extensive knowledge of the calendering process is gathered including the investigation of the displacement behavior for both the calender rolls and the bearing, as well as the adhesion strength. The process parameters such as roll temperature and velocity, structure parameters (e. g., coating thickness, adhesion strength), and machine behavior parameters (displacement and bending line) are investigated using three calender models. The achieved porosities are verified via porosity consistency measurements. Based on the collected data, qualitative machine/material–process–structure models are built up. Scanning electron microscopy (SEM) and light microscopy support the relations made. In addition, a connection between vertical displacement and line load is established.

1. Introduction

The change in transport sector from combustion engines to battery electric vehicles and the growth in portable applications will increase the demand for batteries in the coming years.[1,2] Energy density is a very important property of battery cells and special attention to the compaction process should be given.[1,3,4]

D. Schreiner, M. Oguntke, T. Günther, Prof. G. Reinhart
Institute for Machine Tools and Industrial Management
Technische Universität München
Boltzmannstr. 15, 85748 Garching, Germany
E-mail: david.schreiner@iwb.mw.tum.de

The ORCID identification number(s) for the author(s) of this article can be found under https://doi.org/10.1002/ente.201900840.

After coating and drying, the electrodes have a high porosity. To increase the volumetric energy density, the electrodes are compressed to a lower porosity during calendering.[5]

However, there is a conflict of objectives in the selection of the target porosity between good ionic conductivity (high porosity)[6–8] and high electrical conductivity (low porosity).[6,7,9–11] To resolve this conflict, a specific porosity is calendered, which represents the best possible compromise between the two properties described.[12,13] Output parameters of each subprocess of battery production are simultaneously the input parameters for the subsequent process step due to the linear production sequence (see **Figure 1** on the left).[4,14–16] Prior to calendering, the mechanical properties are affected by the substrate foil and coating thickness.[14] In addition, the volume fractions of the materials, particle size and shape[14] as well as the mixing procedure from upstream processes are affecting these characteristics.[4]

In addition to the preliminary processes of mixing, coating, and drying, the calendering process decisively influences the mechanical[6,17] and electrochemical properties of the electrodes[9] (Figure 1 on the right).

The mechanical homogenization through calendering[17] leads to a homogeneous aging of the cell[17,18] and results in a lower standard deviation of the discharge capacities.[18] This can be explained by lower inhomogeneities within the particle-pore structure at higher densities.[19] Calendering is also important to reduce product quality deviations in terms of C-rate performance.[18,20] Investigations of lithium iron phosphate (LFP)-cathodes have shown that the influence of densification increases significantly with higher C-rates as well as rising number of cycles. The compacted LFP-cathodes have a lower capacity loss over the number of cycles compared with the uncalendered counterpart.[20] An analysis of the pore structure by mercury porosimetry shows that compressing cathodes leads to smaller pore sizes.[21] The tighter particle structure can be attributed to the mechanical stresses applied during the compaction process which lead to a rearrangement of the particles.[16,22] The porosity determined during calendering strongly affects the wetting behavior and thus the wetting time of the electrode.[23]
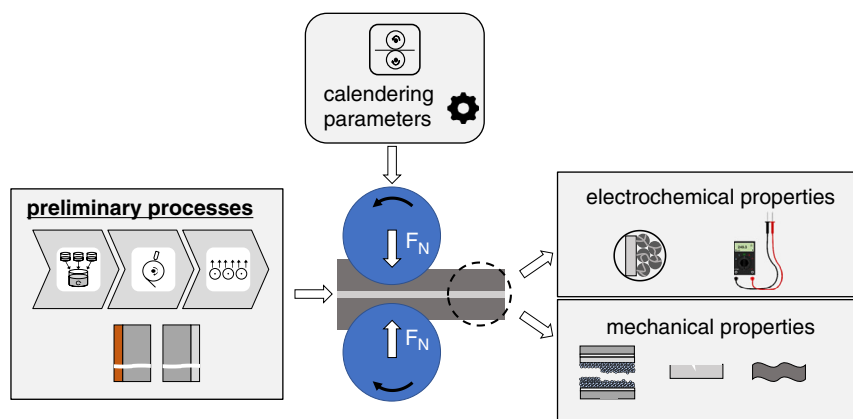
Figure 1. Electrochemical and mechanical properties of the calendered electrodes as a function of the electrode properties from preliminary processes and the selection of calendering parameters.

To achieve higher energy densities, a further reduction of the amount of inactive materials such as substrate foil, binder, and housing is required.[24] This can be accomplished with larger cell formats[24] and thicker electrodes.[25] To increase adhesion strength for thicker electrodes, the mechanical properties of the electrode will become increasingly relevant.[26,27] The adhesion strength of graphite anodes is mainly influenced by the binder content and the coating thickness; calendering further alters the adhesion strength.[28] A higher adhesion strength can be achieved by lower porosities, larger roll diameters, and roll tempering.[28] However, to our knowledge, the mechanical effects of calendering are scarcely considered in the literature. In a previous publication, the authors showed how the mechanical properties of electrodes influence the production process by collecting the defects during calendering and investigating their causes.[22]

As the coating of anode and cathode generally varies in their material properties, both electrodes show a different calendering behavior.[12,13] Cathode-active material particles are harder than the anode ones, therefore higher forces must be applied to cause deformation in form of particle–particle rearrangements associated with particle friction.[13]

As indicated in the literature, the porosity determines the area of application of the lithium-ion cell in addition to the materials used.[18] In previous works, the machine behavior was not taken into account although the porosity differs depending on the condition of the electrode before calendering, on the machine behavior of the calender as well as on the selected process parameters. Since the calender rolls are in direct contact with the electrodes, it is important to consider the machine as a further influencing factor in addition to the other process parameters mentioned. The aim of this article is to develop machine/material–process–structure models for vertical and horizontal displacement, adhesion strength properties and line load, respectively. The presented models are intended to explain the correlations of the calendering parameters, the machine behavior, and the structural parameters of the electrodes in relation to the measurement results. This will contribute to a deeper understanding and optimization of the calendering process. Additionally, the scrap rate is reduced, thereby supporting the production of lithium-ion battery cells at lower cost.

2. Results and Discussion

2.1. Displacement Results

For each measurement based on the methodology shown in the Experimental Section of this article, a displacement curve (see **Figure 2**) was obtained. In the beginning, before calendering and in a freely rotating status, the displacement is zero. After a cathode sheet is inserted into the gap, the displacement rises to its maximum and stays about the same until the end of the sheet. The latter is also the end of the compaction process. It turned out that there is a characteristic displacement curve for each calender model. As shown in Figure 2, calender 1 delivers consistently higher displacements than calender 2. The reason for this correlation is, on the one hand, the stiffer mounting of calender 2 due to the shorter travel distances of the upper roll. On the other hand, the two models investigated have different hydraulic units. Furthermore, the roll-bending system of calender 2 counteracts the formation of a bending line.[13] A uniqueness of calender 2
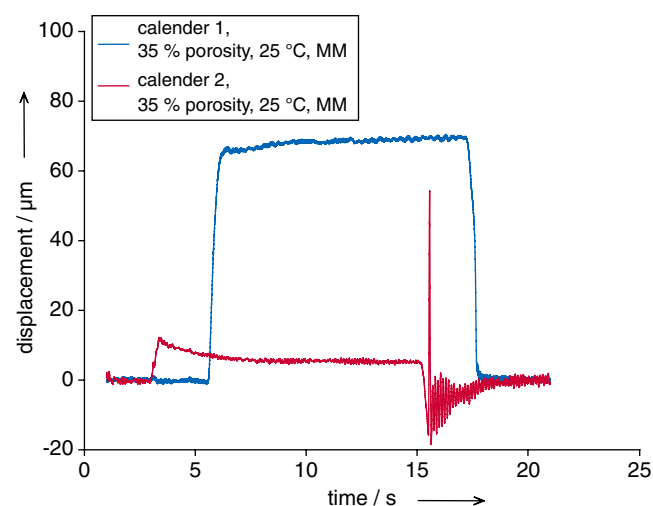
Figure 2. Characteristic displacement curves for calender 1 (with pressure control and without electro-hydraulic gap control) and calender 2 (without pressure control and with electro-hydraulic gap control).

is the overshoot of the curve at the outlet of the electrode sheet. This is due to the electro-hydraulic gap control: The gap width which leads to the target porosity is adjusted via the hydraulic cylinder. Normally, the forces between the electrode in the gap and the roll bending cylinders are in balance during calendering. For the case without an intervention of the gap control, there would be a roller contact as soon as the sheet leaves the gap. To prevent this, the top roller is suddenly moved upward which is noticeable as a short-term deflection in the measurement curve.

First, the results for the vertical displacement of the upper roll at both calender models are presented. Afterward, the outcomes for the horizontal shift are described.

Overall, an increasing compaction (lower target porosity) results in higher vertical displacements. This can be shown for both machines, all investigated temperatures and for both kind of cathodes. Additionally, the attachment of the electric drive affects the displacement at the bearing point which is constantly lower.

Figure 3 shows the vertical displacement curves during the cathode sheets' compaction at calender 2 for three different roller speeds.
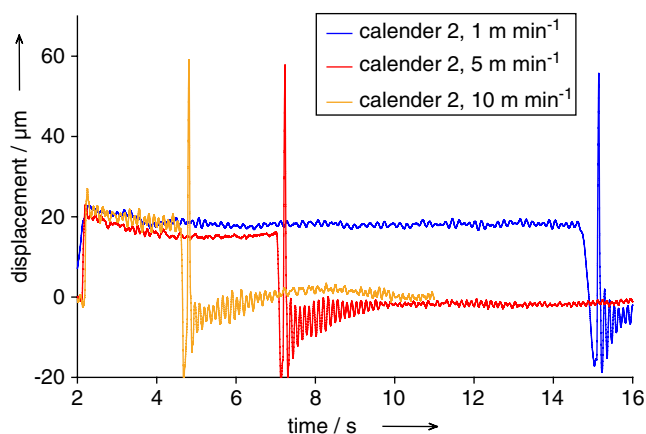

Figure 3. Impact of the roller speed on the vertical displacement at calender 2 with electro-hydraulic gap control.

The measurements were carried out at room temperature (RT), at the roll center and for calendering to 25% target porosity. The figure indicates that the differences in the shift between 1, 5, and 10 m min^{-1} are negligible. Thus, it can be concluded that the speed of the calender rolls in pilot lines has no effect on the displacement in the investigated range. Previous works have shown the same correlation for line load and velocities up to 5 m min^{-1}.[13]

Another important aspect is the relation between roller temperature and displacement. **Figure 4** shows the displacements for the roll center at calender 2 for all porosities investigated as well as the standard deviations. The different curves show the results for RT, 40 and 90 °C. For easier readability, the measured data points of the line load were connected. The standard deviation of the line load is so minimal that it is hardly visible in this graph. It can be stated that lower displacements occur for increasing roller temperatures. Considering the standard deviations, this applies along all compaction rates. For heated rolls and 40% target porosity, no displacements can be measured due to low compaction in combination with high temperatures. This results in low line loads. In addition, it is also striking that at lower temperatures, the relative effect of calendering is more pronounced. For example, the roller displacement for 30 % target porosity during the temperature rise of 15 °C (RT to 40 °C) drops by approximately 7 μm. In contrast, the temperature rise of 50 °C (40–90 °C) leads to a substantially lower displacement with approximately 2.5 μm. Apart from that, the figure additionally shows the line load in N mm^{-1} for the corresponding measurements. When comparing the curves for displacement and line load, a direct correlation can be seen. Thus, it can be stated that the displacement of the upper calender roll can be validated directly via the line load or the rolling force.

The horizontal displacement of the upper roll arises due to the play of the bearing and calender roll itself. When inserting an electrode into the gap, the upper roller is moved out of its idle position by the mechanical resistance and the rolling torque. This results in the formation of a resulting force which leads to the measured horizontal displacement. After the electrode sheet has left the gap, the roller returns to the idle position.
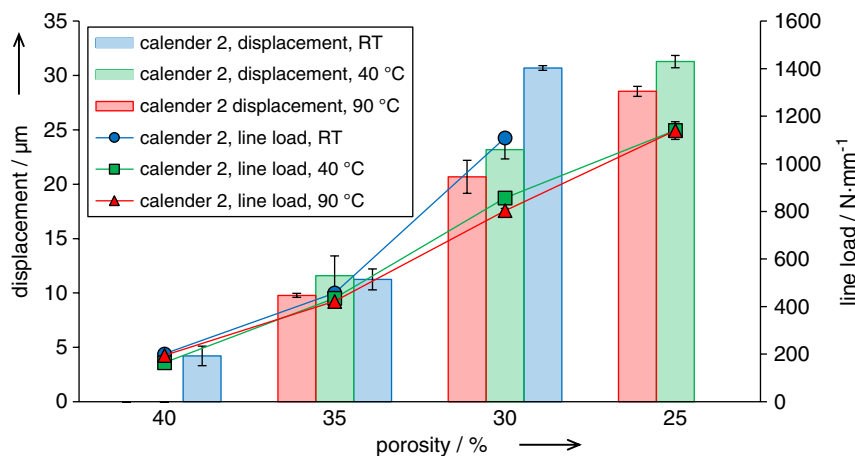

Figure 4. Effects of rising roller temperatures on the displacement of the upper roll and the line load along different target porosities at calender 2.

**ADVANCED
SCIENCE NEWS**

www.advancedsciencenews.com

Energy Technology
Generation, Conversion, Storage, Distribution

www.entechnol.de

The outcomes show that the horizontal displacements are constantly higher at calender 1. At calender 2, there is almost no deflection of the upper roll for any investigated target porosity. The horizontal displacement behavior is therefore, generally analogous to the vertical one but more pronounced. The reason for this relation is the aforementioned stiffer bearing of calender 2. The roll deflection at calender 1 is clearly visible for both 25% and 30% target porosity. Furthermore, the bearings at calender 1 displace in the opposite direction compared with the roller. Nevertheless, this is plausible because the bearings can only move contrary to the direction of the sheet due to their technical design. Overall, the formation of a bending line can be confirmed. Its maximum is slightly offset to the left next to the roller center. As a result, the displacement of the upper roll in the direction of the sheet is partially compensated by the opposite movement of the bearings.

2.2. Adhesion Strength

The coating adhesion of electrodes is an important quality feature regarding the operation of the cell and the processing of the electrodes.[14,28] The electrodes described in **Table 1** (see Experimental Section) were tested on three different calenders (see **Table 2**, Experimental Section). The process parameters roll temperature, compaction rate, as well as the resulting porosity were varied. Depending on the calender and the production batch, the porosity was varied from 47% to 20%, in 5% increments. **Figure 5** shows the results of the investigations described previously. For better readability, the measurement data points were connected. The curves are ranked in the legend according to the adhesion strength at the data point of 30% porosity.

To measure the adhesion strength, a pull-off test with a defined procedure[26] is used. The adhesion strength is measured by the pull-off force during the pull-off test and the sample area. All measurement series have a similar curve shape in common. Starting from the pristine electrodes, the adhesion strength generally decreases with calendering. Based on this, the minimum adhesion strength is at approximately 35% porosity. With increasing compaction and thus lower porosity, the adhesion strength rises again.

Table 1. Characteristics of the NMC-622 cathodes used in this study.

	One-sided	Two-sided
Mass fractions in the coating in wt% (density in g cm^{-3})		
Active material (NMC-622)	95.5 (4.74)	95.5 (4.74)
Binder (PVdF 5130)	2.25 (1.70)	1.50 (1.70)
Graphite additives (Acetylene C65)	1.50 (1.66)	2,25 (1.66)
Conductive carbon black (SFG6L)	0.75 (2.36)	0.75 (2.36)
Measured cathode data		
Current collector thickness in μm (d_{foil})	23	20
Electrode thickness in total in μm (d_{tot})	123	142
Electrode width in total in mm	200	325
Coating width in mm	145	285
Coating porosity (uncalendered) in %	39	47
Coating density (uncalendered) in g cm^{-3}	2.68	2.33

Table 2. Characteristics of the three calender models used in this study.

	Calender 1	Calender 2	Calender 3
Roll diameter in mm	400	465	600
Roll width in mm	400	430	600
Max line load in N mm^{-1}	1000	1500	–
Line load measurement	No	Yes	No
Electro-hydraulic gap control	No	Yes	No
Roll bending system	No	Yes	No
Maximum hydraulic pressure in bar	100	200	250
Pressure control	Yes	No	No
Continuous temperature maximum in °C	150	100	115
Manufacturer	Coatema	Saueressig	Breyer
Calender type	EA 102	GKL 400	–
Location	Munich	Braunschweig	Ulm
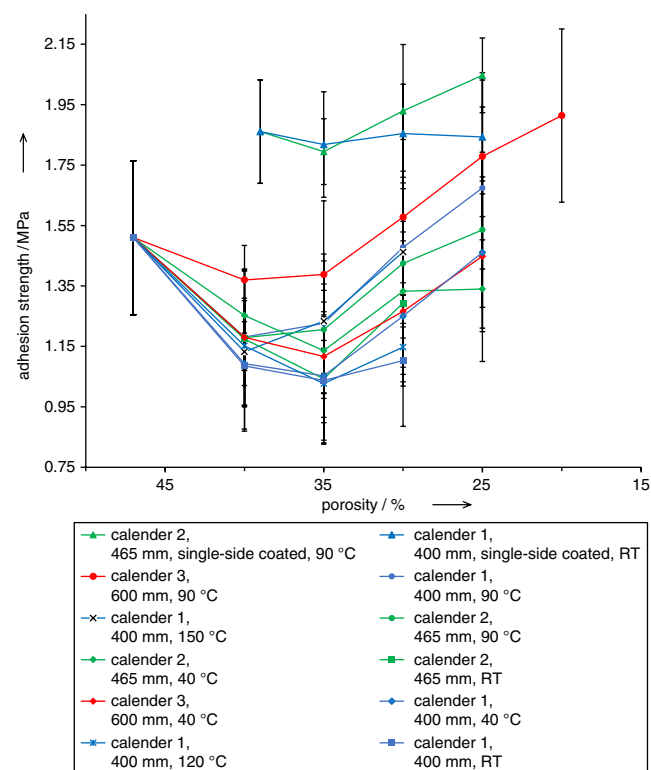
Figure 5. Results of the measurements concerning adhesion strength for different porosities, roller diameters, temperatures, and cathode materials.

In addition, the adhesion strengths of the electrodes from the two different production batches differ considerably. The electrode coated on one side shows higher adhesion strengths than the electrode coated on both sides. This can be attributed to the higher binder content of the single-side-coated electrodes. In addition, the electrodes coated on both sides show a more pronounced improvement in adhesion strengths with increasing roll

temperature. The measurement series with the roll temperature of 90 °C shows a correlation between adhesion strength and roll diameter. Results of additional experiments at calender 1 (blue lines in Figure 5) at 120 and 150 °C confirm the influence of the roll's temperature. Nevertheless, additional tests at calender 1 with temperatures above 90 °C show that higher temperatures do not necessarily lead to higher adhesion strengths. At 120 °C, a decrease in the adhesion strength values can be observed.

For further heating and calendering at a roll temperature of 150 °C, the adhesion strength values return to levels similar to 90 °C. A possible explanation for this observation might be that the compaction behavior of PVDF is a function of temperature and force (see also Figure 4).

The curve described previously corresponds to the graph shown in the literature and has already been explained.[11,28,29] The shear stress between the roller and electrode bonds the interface between substrate and coating at low compaction rates. At higher compaction rates, the adhesion strength increases again, for example by better embedding of the particles in the binder carbon black matrix or by pressing the hard NMC particles into the substrate foil (see **Figure 6**). This explanation is supported by the literature, which shows a continuous increase in adhesion strength of electrodes compacted with uni-axial presses.[30] Furthermore, the observation of particles being pressed into the foil is already confirmed in the literature.[30] Higher roll's temperatures promote the rearrangement of the particles in the binder carbon black network by changing the mechanical properties of the binder. Larger roll diameters reduce the shear stress between the roll and electrode surface and are beneficial to higher adhesion strengths. In the experiments, the roll temperature of 90 °C combined with large roll diameters results in the highest adhesion strengths and is therefore recommended.

As can be seen in the light microscope images at the top of Figure 6, calendering of the electrode reduces its thickness from 142 μm at 47% to 112 μm at 30% porosity and causes particles to be pressed into the substrate foil (see red marks). The scanning electron microscopy (SEM)-images at the bottom of Figure 6 indicate that particle rearrangement due to calendering to

30% has occurred. In addition, a surface smoothing of the calendered electrode can be observed. This is accompanied by particle deformation and particle fragmentation. If the temperature is increased to 150 °C during calendering, the particle surface continues to smoothen.

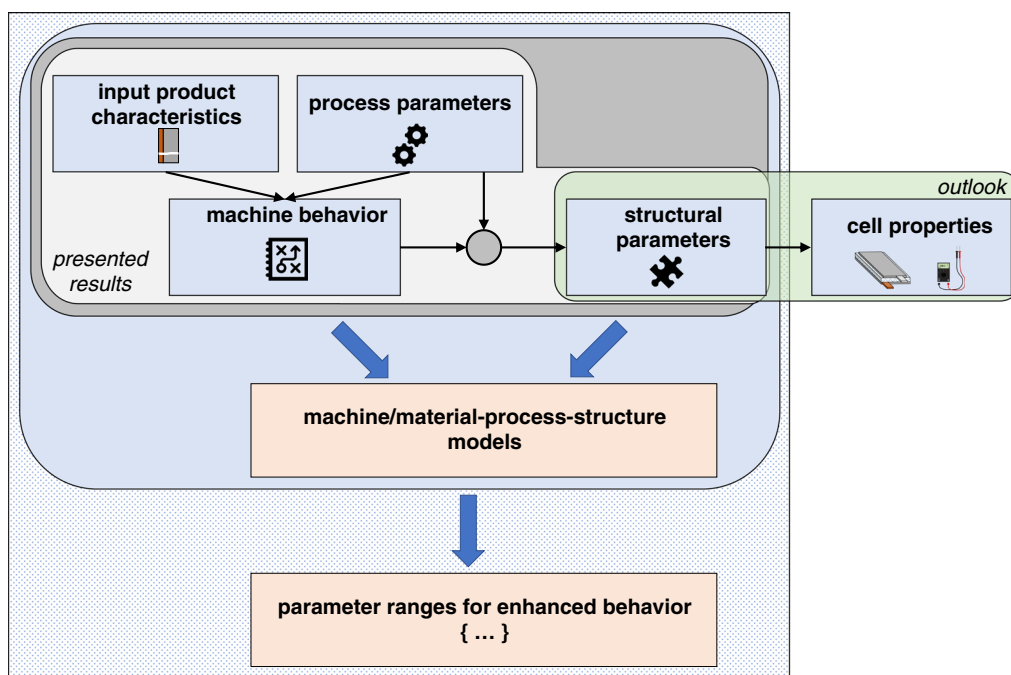## 2.3. Data Conversion into Machine/Material–Process–Structure models

In this section, the interactions between the structural properties, machine behavior caused by the input product characteristics, and the process parameters are introduced. This is performed with reference to the previously presented results of the examined NMC-622 cathodes. **Figure 7** shows the objective, scope, and development procedure of the machine/material–process–structure models, which is outlined more precisely in the following paragraph. The models are based on a graphic description of the correlations.

This article focuses on the correlation between the process and structural parameters of the cathodes and the machine behavior of the calender. These are summarized in **Table 3** and transferred to the previously mentioned models. Additionally, the structural parameters influence the electrochemical performance of the cells which will be part of a follow-up article. The parameter ranges for enhanced behavior will also be part of the following article.

Figure 8 shows the machine/material–process–structure model for the vertical displacement. The different line colors purely are for easier understanding of the interrelations. As explained before, the deflection of the roll due to calendering is composed of horizontal and vertical displacement. This is taken into account in the visualization by the tags "interface" (white square) and "sub" (subobject of the displacement). The following parameters have a significant effect on the vertical displacement behavior: 1) bearing arrangement, depending on the calender model; 2) coating thickness (type of coating application); 3) roll temperature; and 4) porosity and compaction rate.
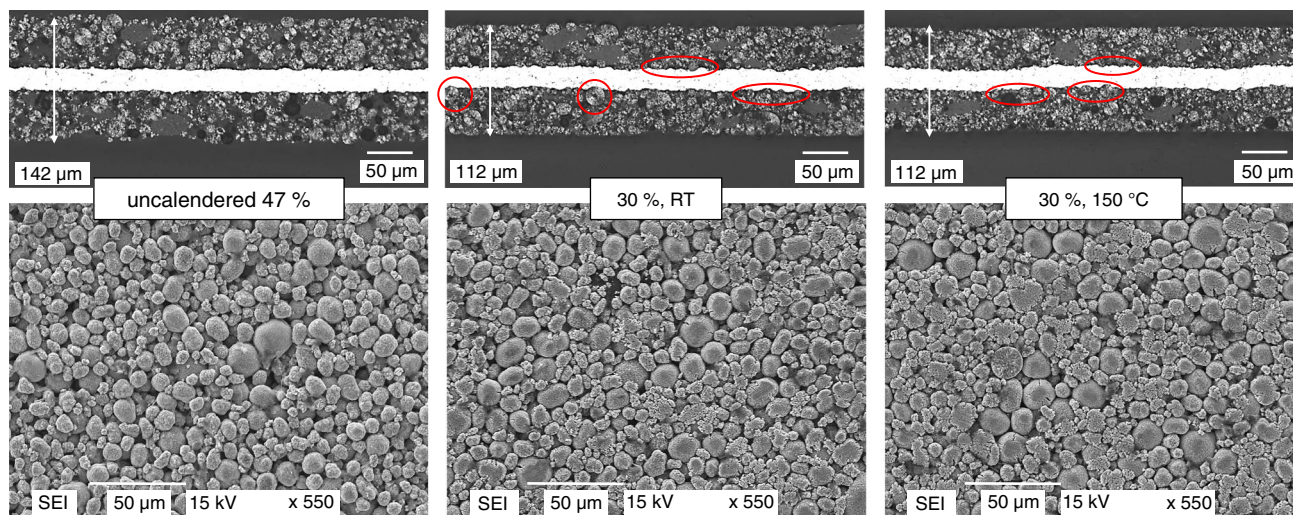
Figure 6. Changes in the particle structure of an NMC-622 cathode due to calendering. Transverse section by light microscopy (top) and surface morphology by SEM (bottom) for different porosities and roll temperatures, respectively.

**ADVANCED
SCIENCE NEWS**

www.advancedsciencenews.com

Energy Technology
Generation, Conversion, Storage, Distribution

www.entechnol.de

Figure 7. Description of the scope and procedure for creating the machine/material–process–structure models.

Table 3. Investigated process, structure, and machine behavior parameters.

|	Parameters
Process	Calender setup (roll diameter, bearing arrangement, operating principle, hydraulic unit)
	Roll temperature
	Roll velocity
	Rolling force and line load
	Compaction rate
Structure	Coating thickness (type of coating application)
	Initial porosity
	Adhesion strength
	Thickness variation (or homogeneity)
Machine behavior	Dynamic behavior:
	Vertical and horizontal displacement
	Formation of a roll bending line

The analysis of the measurement results revealed a direct correlation between decreasing vertical displacements (displayed as "−" in the figure) and increasing porosities (conterminous to decreasing compaction rates, indicated by "+" at the other end of the line). These two parameters are also subject to a further formal precondition: To be able to build up the model, the porosity (compaction rate) is fixed to the highest (lowest) investigated value (as indicated in the yellow mark and the phrase "set"). This is passed on to the roll temperature as an input variable. For rising roll temperatures, decreasing vertical displacements can again be observed. However, the roll temperature is negligible for low compaction rates. In addition to the roll temperature, the relative increase is also noticeable in the displacement values. For lower temperature increases (from RT to 40 °C), the values decrease significantly more than for higher temperature increases (from 40 to 90 °C). The influence of the bearing, depending on the respective calender model, is more obvious: For a higher bearing stiffness χ, the vertical displacement decreases significantly. Compared with a conventional bearing, a roll bending system is advantageous due to the counter-bending of the rolls. The relation concerning the coating thickness (type of coating application) is as follows: as the coating thickness decreases, the vertical displacement declines as well.

There are further indirect relationships, characterized by the dotted connecting lines in the model. The roller speed was examined as a parameter (1, 5, and 10 m min^{-1}), but the experiments showed it has no effect on the displacement behavior. Basically, the vertical displacement is lower on the side to which the electric drive is attached. However, this is a local phenomenon at the bearing and does not influence the displacement at the five measurement points. Therefore, it represents an indirect correlation in the model. Furthermore, force measurements at calender 2 showed that the vertical displacement correlates with the line load. Since the latter is a separate expression of the machine behavior, this relation is represented in the model by the connection with an environmental interface (white square).

In **Figure 9** the interrelations between the adhesion strength and the following parameters are displayed: 1) porosity and compaction rate; 2) coating thickness (type of coating application); 3) binder content; 4) roll temperature; and 5) roll diameter, depending on the calender model.

The graphic clearly shows that adhesion strength increases for lower porosities and higher compaction rates. However, this only
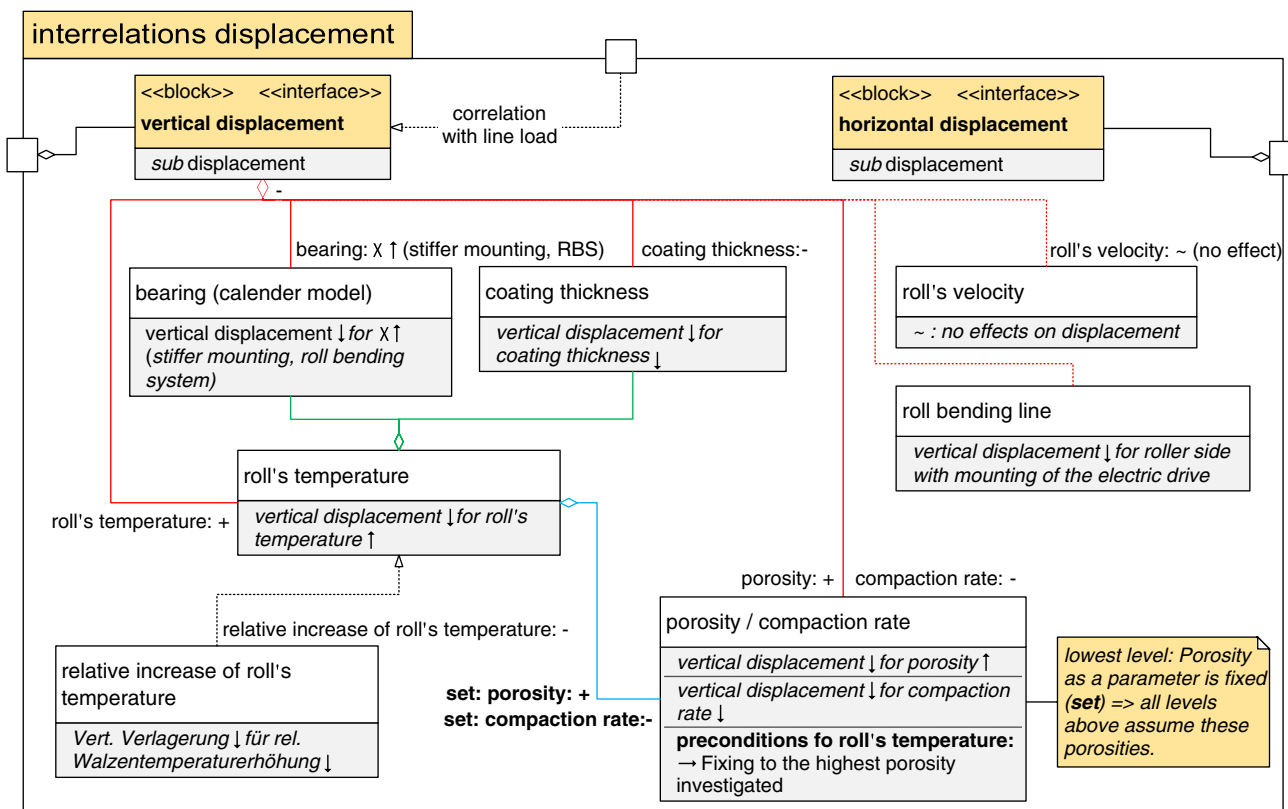
Figure 8. Machine/material–process–structure model for the vertical displacement behavior of the upper calender roll.

applies under the precondition that the low point of the trough-shaped curve has already been passed. Before this, the adhesion strength values decrease continuously up to a certain porosity with increasing compaction. Afterward, the trend reverses and comes to a global maximum. Furthermore, thinner coating thicknesses are advantageous because the number of possible failure mechanisms in the composite or between coating and foil is limited. A higher binder content also improves adhesion strength.[28] Another detected parameter is the roll temperature. In general, the temperature for easy deformability should be close to the melting point (150 °C for PVdF[31]) and therefore be as high as possible.
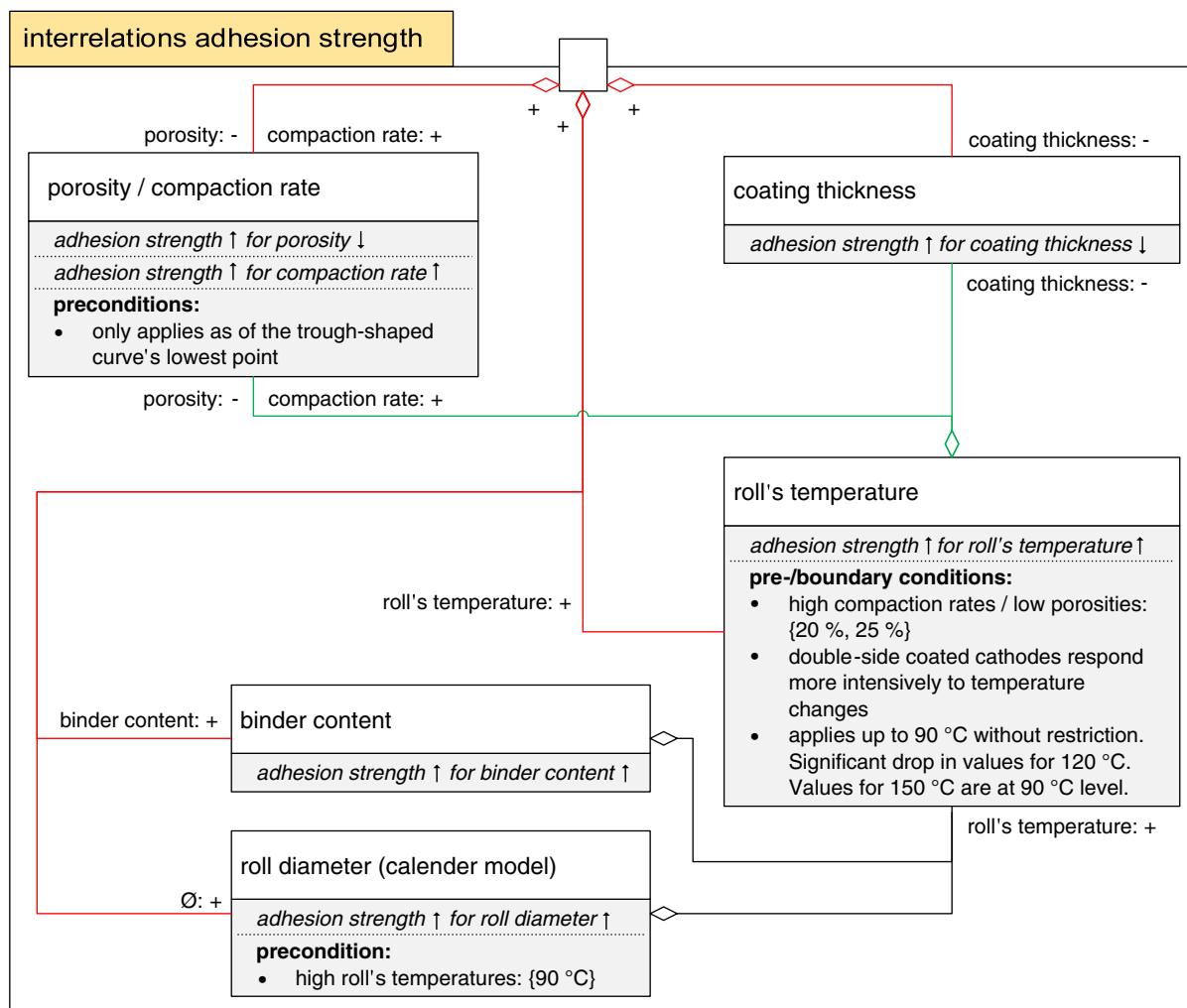
The results of this work show that adhesion strength generally increases with rising temperature. Above 90 °C, a deviating ambiguous behavior was observed. For 120 °C, the adhesion strength drops significantly, and for 150 °C, the values reach the level of 90 °C. Additionally, two further preconditions must be considered: first, a high compaction rate must be used. Second, the examined cathodes coated on both sides react more strongly to temperature changes than cathodes coated on one side. This is due to the lower relative coating thickness of the cathode with double-sided coating. Under the precondition of high roll temperatures, larger diameters also lead to a higher adhesion strength (90 °C turned out to be optimal during the tests). As shown in a previous publication for anodes,[28] the binder content also affects the adhesion strength for cathodes. From the experiments carried out within the framework of this

article, it is evident that an increase in binder content from 1.5 to 2.25 wt% leads to a pronounced increase in adhesion strength. Thus, improvements can be achieved with a small amount of additional binder. In addition, adhesion strength of the investigated NMC-622 cathodes can be enhanced by increasing the roll temperature without further addition of binder. This temperature-dependent improvement in adhesion strength can be beneficial especially for thick electrodes, where adhesion strength normally decreases.[28] Thus, a higher adhesion strength can be achieved with the same amount of active material through optimized process parameters, leading to an increase in the ratio of adhesion strength to energy density.

The machine/material–process–structure model for the line load will be presented in a follow-up study.

3. Conclusions

As stated in the Introduction, it is essential to make progress in the related production technology to further enhance battery technology. A profound and deep process understanding, as well as knowledge concerning the dependencies between the individual parameters and process steps support this development. In summary, machine/material–process–structure models were built up for the calender's machine behavior and the structural properties of the NMC-622 cathodes. Therefore, process and structural parameters were correlated using data from a

ADVANCED
SCIENCE NEWS

www.advancedsciencenews.com

Energy Technology
Generation, Conversion, Storage, Distribution

www.entechnol.de

Figure 9. Machine/material–process–structure model for the adhesion strength of the NMC-622 cathodes investigated.

structured DoE multitude of experiments. During the investigations, different calender models as well as cathodes with single- and double-sided coating were analyzed. In addition, dependencies between the parameters were determined and mapped in the model. The subsequent machine/material–process–structure model for vertical displacement shows direct correlations between bearing (dependent on calender model), coating thickness, roll temperature, and porosity/compaction rate. Apart from that, the roll velocity on the pilot line between 1.0 and 10 m min^{-1} has no effect on the displacement in the investigated range at calender 2. The roller side with mounting of the electric drive shows a lower vertical displacement, resulting in a roll bending line. Furthermore, the relative increase of roll temperature is an indirect correlation on the vertical displacement and line load (see Figure 4 and 8), since the roll temperature is the main parameter.

The model concerning rising adhesion strength shows direct influence of decreasing porosity/increasing compaction rate, decreasing coating thickness, increasing binder content, increasing roll temperature, and increasing roll diameter

(depending on the calender model). Furthermore, SEM-images support the statements made. To be precise, the first dependency mentioned applies after the lowest point (35% porosity) of the trough-shaped curve. During statistic review, the plausibility of the data was verified. These results extend the state of the art and help to understand the calendering process in depth. In addition, the models presented can be used to achieve electrodes which more predictably meet the desired requirements.

The presented data for vertical displacement shows that the true gap distance is changing during the process. This appears especially for changes of the electrode thickness, e.g., at the beginning and end of the coating. Further investigations could make it possible to transfer the models into a database with a Graphical User Interface. The goal should be that the user enters the desired product properties and is instructed with the parameters to be set at the machine. With measuring the real gap, the elastic relaxation of the electrode can be determined. Furthermore, the cathodes' electrochemical properties will be analyzed in a follow-up article.

4. Experimental Section

The Experimental Section covers the presentation of the calender models and the investigated electrodes. Furthermore, the methodology of the displacement measurements and the porosity consistency verification are introduced.

Calender Models: The electrodes were compacted using different calenders to investigate the differences in machine behavior (see Table 2). In the pilot line[32] at the Institute for Machine Tools and Industrial Management (iwb) at the Technical University of Munich (TUM), the model EA 102 from Coatema Coating Machinery GmbH (calender 1) was used.[33] The same machine was used for investigations concerning electrode defects.[22] The diameter of the two identical rolls was 400 mm with the same width. Two independent electric motors allow path velocities of 0.1–3.0 m min^{-1}. The maximal applicable line load was 1000 N mm^{-1} along an operating width of 300 mm. By manually varying the gap size between the rolls, different line loads were applied. In addition, the rolls could be tempered by means of an externally heated thermal oil. The maximum achievable roller temperature is 150 °C. To investigate the correlation between the calender roll displacement and the line load, a force measurement was retrofitted. It was technically based on the measurement of the upper rolls' back pressure. The applied line load (q_L) was calculated from the rolling force (F_N) and the coating width (w_C) of the cathode: $q_L = F_N / w_C$.[13]

The second calender model investigated was GKL 400 from Saueressig GmbH & Co. KG (calender 2) and used at the Institute for Particle Technology (iPAT) at Technical University of Braunschweig (TUB).[13] An overview concerning important machine data of the different calender models is collected in Table 2.

For adhesion strength investigations, the calender of the research production lines (FPL) at Center for Solar Energy and Hydrogen Research Baden-Württemberg (ZSW) in Ulm was added to the calenders already described. It was manufactured by Breyer Extrusion GmbH and had a roll diameter and width of 600 mm (calender 3).

Electrode Materials and Composition: In this article, two different NMC-622 cathodes were used. Though they are based on the same amount and kind of components, they were made in different campaigns within the Competence Cluster for battery cell production (ProZell)[34] and differ in the type of coating application (single or double sided). Detailed specifications of the coating materials and the measured cathode data are denoted in Table 1.

To carry out the displacement measurements, the coiled cathode material was separated into single sheets of 210 mm ± 10 mm. During the investigation of different speeds, longer sheets were used for higher rolling velocities due to the handling requirements. The cathode's porosity is calculated as follows[12]

$$\phi = 1 - \frac{V_{th}}{V_m} = 1 - \frac{\sum_{i=1}^{n} V_i}{A_{sheet} \cdot d_{coating}} = 1 - \frac{\sum_{i=1}^{n} \frac{m_i \cdot c_i}{\rho_i}}{\left(\frac{s_{punch}}{2}\right)^2 \cdot \pi \cdot (d_{tot} - d_{foil})} \quad (1)$$

To calculate the theoretical volume of the electrode (V_{th}), the volumes (V_i) of the single electrode components need to be determined and added up. For this purpose, the mass (m_i) is multiplied by the respective material content of the coating (c_i) and then divided by its density (ρ_i). The measured volume of the electrode (V_m) is determined by multiplying the area of a punched-out, round cathode piece (A_{sheet}), and the thickness of the coating ($d_{coating}$). The former is calculated from the known punching diameter (s_{punch}). The latter results from the difference between the total electrode thickness (d_{tot}) and the thickness from the collector foil (d_{foil}).

As part of the calendering process, setting the target porosity of the cathodes is done indirectly via the compaction rate Π. It describes the percental change in the electrode thickness due to the calendering process. The compaction rate can be calculated as follows[17]

$$\Pi = 1 - \frac{d_{E,cal}}{d_{E,initial}} \quad (2)$$

The parameter $d_{E,cal}$ describes the electrode thickness after the calendering process and $d_{E,initial}$ describes the thickness of the noncompressed electrode.

Methodology of the Displacement Measurements: The displacement measurements are carried out using laser Doppler vibrometry. In principle, the measuring technique analyzes the Doppler effect on a laser beam reflected from a moving surface.[35] The direct measurement of the target's displacement is based on counting the light–dark transitions on the detector.[36]

For measuring the horizontal displacement and the vertical one at calender 2, the single-point laser vibrometer ODV-505 with autofocus from Polytec GmbH was used.[37] The head was fixed on a tripod for an exact adjustment of the height. A correct alignment along the axes of the calender coordinate system was facilitated by spirit levels on the top of the tripod. Additionally, it can be verified using visual inspection through the direct reflection of the laser beam from the calender roll parallel to the lens of the vibrometer.

Due to difficult accessibility, a flexible measuring head was required for measuring the vertical displacement at calender 1. Therefore, the fiber-optic head OFV-552 from Polytec GmbH[38] was used. In contrast to the single-point laser vibrometer, focusing had to be adjusted manually. During the execution of the experiments, especially with heated rolls, the heads' specified operating temperature range of +5 to +40 °C had to be observed.[37,38] The analogue signal from the respective vibrometer was prefiltered by the controller box OFV-5000 to suppress static noise.[39] The split signal was transferred to a BNC-USB converter via the velocity
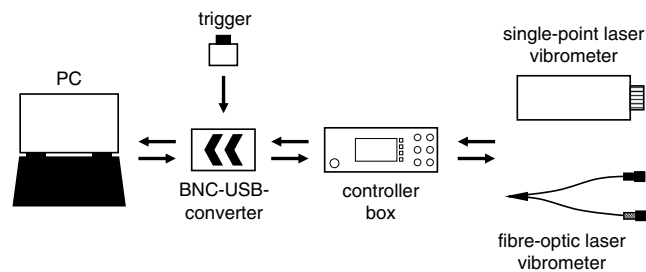
Figure 10. Methodology of the displacement measurements.

Table 4. Vertical displacement measurement data for various porosities, temperatures, and calenders using the single-side-coated (black) and the double-side-coated (light blue) cathodes.

Temperature porosity *in* %	RT					40 °C					90 °C				
	40	35	30	25	20	40	35	30	25	20	40	35	30	25	20
Calender 1		✓	✓				✓	✓	✓						
		✓	✓	✓											
Calender 2	✓	✓	✓			✓	✓	✓			✓	✓	✓	✓	
		✓	✓	✓								✓	✓	✓	

and displacement output channels. Finally, the data were transmitted to the PC (see **Figure 10**). The start of the measurement is released via the trigger and the iwb FRF-Tools software. To monitor the standard deviation, each measurement is repeated three times. During the evaluation, the average between the absolute displacement at the in- and outlet of the cathode sheet is determined and transmitted to an Excel sheet.

Furthermore, it is important to decouple the measuring devices from vibrations. Since the tripod and so the single-point laser vibrometer are in direct contact with the floor, conical rubber buffers were attached. The fiber optic laser vibrometer can be considered as vibration-decoupled due to the attachment of the head in the fixture.

At calender 1 and 2, five measuring points along the upper roll were investigated: C is in the center of the roll. R and L are located on the right and left, respectively, with 20 mm to the end of the roller. CL and CR are situated in the middle between the center and the outer points. The five measurement locations allow the vertical and horizontal roll deflection to be determined. In addition, BL and BR are located left and right in the middle of the bearings, respectively. **Table 4** shows the executed vertical displacement measurement data. The results are subdivided according to porosity, roll temperature, and calender models. Empty cells are due to the limitation of the adjustable minimum gap width, the maximum hydraulic pressure, and limitations of the materials' availability. Apart from that, limitations of the heads' specified operating temperature had to be observed.

Methodology of the Porosity Consistency Verification: Measuring the thickness of the calendered cathodes was necessary to check the homogeneity of the target porosity. This is an important point to secure the quality of the calendered electrodes. The setup consists of the measurement sensor ID-C112AX (Mitutoyo GmbH) which is attached to a joint rod structure and placed on a granite plate. The dial gauge's accuracy is $\pm 1\,\mu m$.[40] To state the change in thickness across the electrode, the measurement points on each cathode sheet were arranged as follows: 20 measurement points over the length with three rows across the width provided a good compromise between effort and accuracy.

Supporting Information

Supporting Information is available from the Wiley Online Library or from the author.

Conflict of Interest

The authors declare no conflict of interest.

[1] C. Meyer, M. Kosfeld, W. Haselrieder, A. Kwade, *J. Energy Storage* **2018**, *18*, 371.

[2] a) Y. Ding, Z. P. Cano, A. Yu, J. Lu, Z. Chen, *Electrochem. Energ. Rev.* **2019**, *2*, 1; b) Y. Lu, Q. Zhang, J. Chen, *Sci. China Chem.* **2019**, *192*, 1126.

[3] R. Schmuch, R. Wagner, G. Hörpel, T. Placke, M. Winter, *Nat. Energy* **2018**, *3*, 267.

[4] A. Kwade, W. Haselrieder, R. Leithoff, A. Modlinger, F. Dietrich, K. Droeder, *Nat. Energy*, **2018**, *3*, 290.

[5] D. L. Wood, J. Li, C. Daniel, *J. Power Sources*, **2015**, *275*, 234.

[6] H. Zheng, L. Tan, G. Liu, X. Song, V. S. Battaglia, *J. Power Sources*, **2012**, *208*, 52.

[7] Y.-H. Chen, C.-W. Wang, X. Zhang, A. M. Sastry, *J. Power Sources*, **2010**, *195*, 2851.

[8] Z. H. Li, H. P. Zhang, P. Zhang, G. C. Li, Y. P. Wu, X. D. Zhou, *J. Membr. Sci.* **2008**, *322*, 416.

[9] C.-W. Wang, Y.-B. Yi, A. M. Sastry, J. Shim, K. A. Striebel, *J. Electrochem. Soc.* **2004**, *151*, A1489.

[10] G.-F. Yang, S.-K. Joo, *Electrochim. Acta*, **2015**, *170*, 263.

[11] C. Schilcher, C. Meyer, A. Kwade, *Energy Technol.* **2016**, *4*, 1604.

[12] M. K. Gulbinska, *Lithium-ion Battery Materials and Engineering*, Springer, London, **2014**.

[13] C. Meyer, H. Bockholt, W. Haselrieder, A. Kwade, *J. Mater. Process. Technol.* **2017**, *249*, 172.

[14] T. Günther, N. Billot, J. Schuster, J. Schnell, F. B. Spingler, H. A. Gasteiger, *AMR*, **2016**, *1140*, 304.

[15] M. Westermeier, G. Reinhart, M. Steber, *Proc. CIRP*, **2014**, *20*, 13.

[16] H. Bockholt, M. Indrikova, A. Netz, F. Golks, A. Kwade, *J. Power Sources*, **2016**, *325*, 140.

[17] W. Haselrieder, S. Ivanov, D. K. Christen, H. Bockholt, A. Kwade, *ECS Trans.* **2013**, *50*, 59.

[18] G. Lenze, H. Bockholt, C. Schilcher, L. Froböse, D. Jansen, U. Krewer, A. Kwade, *J. Electrochem. Soc.* **2018**, *165*, A314.

[19] H. Kang, C. Lim, T. Li, Y. Fu, B. Yan, N. Houston, V. de Andrade, F. de Carlo, L. Zhu, *Electrochim. Acta*, **2017**, *232*, 431.

[20] C. F. Oladimeji, P. L. Moss, M. H. Weatherspoon, *Adv. Chem.* **2016**, *2016*, 1.

[21] L. Froboese, P. Titscher, B. Westphal, W. Haselrieder, A. Kwade, *Mater. Charact.* **2017**, *133*, 102.

[22] T. Günther, D. Schreiner, A. Metkar, C. Meyer, A. Kwade, G. Reinhart, *Energy Technol.* **2019**.

[23] J. B. Habedank, F. J. Günter, N. Billot, R. Gilles, T. Neuwirth, G. Reinhart, M. F. Zaeh, *Int. J. Adv. Manuf. Technol.* **2019**, *273*, 966.

[24] D. Andre, S.-J. Kim, P. Lamp, S. F. Lux, F. Maglia, O. Paschos, B. Stiaszny, *J. Mater. Chem. A*, **2015**, *3*, 6709.

[25] A. Sakti, J. J. Michalek, E. R. H. Fuchs, J. F. Whitacre, *J. Power Sources*, **2015**, *273*, 966.

[26] W. Haselrieder, B. Westphal, H. Bockholt, A. Diener, S. Höft, A. Kwade, *Int. J. Adhes. Adhes.* **2015**, *60*, 1.

[27] S. Jaiser, N. Sanchez Salach, M. Baunach, P. Scharfer, W. Schabel, *Drying Technol.* **2017**, *35*, 1807.

[28] N. Billot, T. Günther, D. Schreiner, R. Stahl, J. Kranner, M. Beyer, G. Reinhart, *Energy Technol.* **2019**.

[29] W. Haselrieder, PhD Dissertation, Technische Universität Braunschweig, **2016**.

[30] H. Y. Tran, G. Greco, C. Täubert, M. Wohlfahrt-Mehrens, W. Haselrieder, A. Kwade, *J. Power Sources*, **2012**, *210*, 276.

[31] Arkema Inc., Performance Characteristics & Data Polyvinylidene Fluoride. Kynar/Kynar Flex, **2016**.

[32] G. Reinhart, T. Zeilinger, J. Kurfer, M. Westermeier, C. Thiemann, M. Glonegger, M. Wunderer, C. Tammer, M. Schweier, M. Heinz, *Future Trends in Production Engineering. Research and demonstration center for the production of large-area lithium-ion cells* (Eds.: G. Schuh, R. Neugebauer, E. Uhlmann), Springer, Berlin, **2013**, pp. 3–12.

[33] Coatema Coating Machinery GmbH, Gesamtdokumentation Kalander EA102, Dormagen, **2013**.

[34] ProZell, ProZell Kompetenzcluster zur Batterieproduktion. Willkommen bei ProZell, https://www.prozell-cluster.de/ (accessed: July, 2019).

[35] E. Esposito, *Handbook of the use of lasers in conservation and conservation science* (Eds.: M. Schreiner, M. Strlič, R. Salimbeni), COST Office, Brussels, **2008**.

[36] Polytec GmbH, Grundlagen der Vibrometrie, http://www.polytec.com/de/loesungen/schwingungen-messen/grundlagen-der-vibrometrie/ (accessed: July, 2019).

[37] Polytec GmbH, OFV-505 Messkopf. Datenblatt, Waldbronn, **2015**.

[38] Polytec GmbH, OFV-551/552 Fiber-Optic Sensor Head. Datasheet, Waldbronn, **2017**.

[39] Polytec GmbH, OFV-5000 Vibrometer Controller. Datenblatt, Waldbronn, **2016**.

[40] Mitutoyo Corporation, *ID-C112AX User's Manual. ABS Digimatic Indicator with Peak-Value Hold Function*, Kanagawa, Japan, **2015**.